

Spontaneous Emergence of Static Friction Force and Vanishment of Dynamic Friction Force in Slip Front Propagation

*Takehito Suzuki¹, Hiroshi Matsukawa¹

1.Department of Physics and Mathematics, Aoyama Gakuin University

We show spontaneous emergence of static friction force and vanishment of dynamic friction force in the dynamics of slip front propagation with local friction law nonlinearly depending on the slip velocity, which has no static friction force. We consider a block on a substrate and load one side of the block to slide it against the substrate. We take x axis along the loading direction and the block is assumed to be a semi-infinite isotropic homogeneous medium occupying the region $z>0$. The substrate is a rigid plane at $z=0$. The slip of block at $x \rightarrow \infty$ is fixed to be zero and we load the block at $x \rightarrow -\infty$ to initiate the slip. We employ the friction law having a quadratic form of the slip velocity, and derive the steady state solution for the motion of the slip front; the friction force τ is given by $-av^2 + 2abv$, where v is the slip velocity and a and b are constants. With this friction law, the sliding friction force changes from the velocity-strengthening to the velocity-weakening behaviors with increasing slip velocity. This friction law enables us to treat the problem analytically, because the friction force is a single valued function of the slip velocity.

We can obtain the profiles of the slip and the strain of the steady state of the slip front dynamics, which is found to give the relationship between the strain at $x \rightarrow -\infty$ (the loading point) p_{inf} (<0) and the slip front velocity c ; $|p_{inf}|=2b/c$. It is also important to note that c must be smaller than the bulk elastic wave velocity v_e for the existence of the steady state. These statements indicate that p_{inf} has the critical value. If $|p_{inf}|<2b/v_e$, the steady propagation cannot be observed and the slip amplitude decays with increasing time. On the other hand, if $|p_{inf}|>2b/v_e$, the steady propagation of slip appears. These behaviors imply spontaneous emergence of the static friction force even though the local friction has no static friction force. Macroscopic static friction force is given by $2bE_1/v_e$, where E_1 is the Young modulus.

The analytical result obtained in the present study also indicates the slip velocity at $x_1(=x-ct) \rightarrow -\infty$ is $2b$, which results in that the friction force at the loading point in the steady state vanishes since τ is zero with $v=2b$. The dynamic friction force in the steady state is concluded to vanish spontaneously at $x_1 \rightarrow -\infty$.

Keywords: Static Friction Force, Dynamic Friction Force, Nonlinear Friction Law, Analytical Solution, Slip Front Propagation

An arithmetic approach for modeling of seismic activity, No.2

*Hiroyuki Fujiwara¹

1.National Research Institute for Earth Science and Disaster Prevention

An arithmetic seismic activity model is proposed by Fujiwara (2014). In this model, earthquakes are modeled by using prime numbers to express the seismic activity that follows the G-R law. Although the arithmetic seismic activity model has been inferred from phenomenological similarities between seismic activities and the prime number distributions, there may be some mathematical and physical meanings behind the model.

We consider a correspondence between earthquakes and prime numbers. We parameterize occurrence time of earthquakes as prime numbers and magnitude of earthquakes as the interval of prime numbers. Then we obtain a relationship similar to G-R law. We call the model obtained from this correspondence as arithmetic seismic activity model. In the arithmetic seismic activity model, earthquake is equivalent to prime number. Then, earthquake prediction is equivalent to prediction of emergence of prime numbers.

For the prime number distribution, the Riemann explicit formula is known. The Riemann explicit formula is an equation showing the number of primes less than a given number, by using the zeros of the Riemann zeta function. In the arithmetic seismic activity model, the Riemann explicit formula gives a prediction formula of earthquake occurrence.

In this study, for the purpose of giving a physical interpretation to the arithmetic seismic activity model, efforts have been made in the following approach.

- (1) By considering the Riemann explicit formula as a trace formula, we explore the mathematical structure behind it.
- (2) Using the noncommutative geometry and automorphic representation, we challenge to build a dynamic system that can explain the arithmetic seismic activity model.

With respect to (1), the Selberg trace formula, which links geometry and harmonic analysis on a Riemann surface, is known. A common feature in the trace formula, the sum on the prime elements in the geometric side is equal to the sum on the eigenvalues in the spectrum side. Trace formula can be regarded as an equation linking the two different concepts. It is thought to play an important role in mathematical physical modeling. By paying attention to the similarity between the Selberg trace formula and the Riemann explicit formula and by capturing the Riemann explicit formula as a kind of trace formula, it was conducted a survey of the relevant existing research for mathematical structure behind the Riemann explicit formula.

With respect to (2), as a starting point of the above approach, focusing on the similarity between automorphic forms in the field of number theory and mathematical structure of the conformal field theory in the theoretical physics, we have been conducting research towards the construction of the dynamical system. By configuring the dynamical system based on the automorphic form and its representation in an adèle space, we have been conducting preliminary research to capture earthquakes as an eigenvalue problem.

Approach of this study is to construct a bridge linking "prime" as a research subject of number theory and "earthquake" as a physical phenomenon. In the field of number theory, such attempt is known as Langlands program. In recent years, researches to expand the idea of the Langlands program between number theory and theoretical physics has been conducted.

For the prime distribution, historical unsolved problems, such as the Riemann hypothesis, still

exist in number theory. This study is still in the stage of preliminary research towards the resolution of the above-mentioned problems.

References

Hiroyuki Fujiwara (2014): An arithmetic seismic activity model, *Zishin*, vol. 66, 67-71.

Keywords: Number Theory, Prime number, Earthquake, Langlands program

Emergence and disappearance of repeating earthquakes on a geological fault in a deep gold mine in South Africa

*Junya Yamaguchi¹, Makoto Naoi¹, Masao Nakatani², Moriya Hirokazu³, Thabang Kgarume⁴, Toshihiro Igarashi², Osamu Murakami⁵, Thabang Masakale⁶, Yasuo Yabe³, Kenshiro Otsuki³, Hironori Kawakata⁷, Tsuyoshi Ishida¹, Anthony Ward⁸, Ray Durrheim^{4,9}, Hiroshi Ogasawara⁷

1. Kyoto University , 2.The University of Tokyo, 3.Tohoku University , 4.CSIR, 5.Tono Research Institute of Earthquake Science, 6.OHMS, 7.Ritsumeikan University, 8.SeismoGen, 9.University of the Witwatersrand, Johannesburg

We deployed an Acoustic Emission (AE) monitoring network consisting of 30 very sensitive AE sensors and 7 accelerometers at 1-km depth in the Cooke 4 gold mine in South Africa, where many earthquakes up to $M 3$ are induced by stress buildup by mining. Naoi et al. [2015] analyzed data obtained by the AE network during 2 months, and they found very small repeating earthquakes of $-5.1 \leq M_w \leq -3.6$ which occurred on a geological fault. In this study, we extended the analysis period to 14 months, investigating a time variation of the repeating earthquakes during longer periods.

Firstly, we relocated 5869 events that occurred along the geological fault during the 14 months (from 7 April 2011 to 30 May 2012) by using the double-difference method [Waldhauser and Ellsworth, 2000] with the cross-correlation travel-time reading technique. Of the relocated AEs, we chose 3735 events within 3 m from an approximation plane of the two-dimensional distribution of the AEs, which delineates the fault. We then cross-correlated waveforms of all event pairs whose interevent distances D were less than 2 m. We chose event pairs whose seismograms had cross-correlation coefficient greater than 0.90 at 20 percent or more working stations at the time and their rupture areas evaluated from a circular crack model overlapped significantly. We finally assembled them into "repeater groups" whose event pairs shared one event or more. Out of the 3735 events (35.6%), 1328 events belonging to 308 groups were identified as repeaters. The number of recurrence reached 45 times for the largest repeater group.

Activities of some groups continues for the whole 14 months (Type A), but we also found groups that newly emerged (Type B) or disappeared (Type C) in the analysis period. We also found areas of ~ 10 -m scale where only Type-B or Type-C groups existed, which likely corresponds to a newly emerged or terminated macroscopic slow slip respectively. Meanwhile, there were areas where Type A-C existed within a tiny area of a few-meter scale. Only in such area, we found some Type C groups whose events size decreased with time. We consider the emergence and disappearance of the repeaters in such areas represent formation and dissipation of unstable patches of the fault, resulting from newly encountered protruding portions or frictional wear of the contacts by the progress of fault creeping.

Keywords: Acoustic Emission, Induced Earthquake, Repeating Earthquake

Characteristics of Rupture Initiation and Propagation in the Lab

*Eiichi Fukuyama¹, Futoshi Yamashita¹, Shiqing Xu¹, Kazuo Mizoguchi^{2,1}, Shigeru Takizawa¹, Hironori Kawakata^{3,1}

1.National Research Institute for Earth Science and Disaster Prevention, 2.Central Research Institute of Electric Power Industry, 3.Ritsumeikan Univ.

We have conducted large-scale bi-axial shear friction experiments using the NIED large-scale shaking table (e.g. Fukuyama et al., 2014, Yamashita et al., 2015). One of the main targets of these experiments was to investigate the rupture initiation and acceleration process of the stick slip events, which are proxies of natural earthquakes (hereafter, we call them labquakes). The experiments were done under constant loading rate conditions of between 0.01 and 0.1 mm/s under the normal stress of between 1.3 and 6.7 MPa. The rock sample is made of metagabbro from India. We compiled the results obtained in the series of experiments and discuss what we understood and what we need to understand. There are some key observations as follows. 1) We sometimes observed labquakes that did not reach the end of the rock sample. Such labquakes are more similar to the natural earthquakes in a sense that the total stiffness was controlled by the surrounding rock materials. In these events, highest stress drop occurred at the beginning while termination of the rupture was rather gradual. 2) Mainshocks were preceded by the precursory slow slip and/or foreshocks. Sometimes, foreshock activity dominates but in most cases, precursory slip occurred just before mainshocks. 3) The foreshocks tend to be more often observed when the sliding surface was pre-damaged due to previous fast sliding so that more gouge particles were generated under the same loading conditions. 4) After the friction experiment, many grooves were observed on the sliding surface, in which gouge particles were filled. The area where precursory slow slips occur does not have many grooves comparing to the other area, suggesting that slow slip might initiate mainly on the smooth surface where no grooves were created. 5) The hypocenters of the labquakes were located at the edge of the grooves based on the AE sensor array data. This suggests that grooves were created at the initial acceleration stage of the rupture. Based on the above observations, we are constructing the rupture model. And there are several issues that we do not clearly understand. a) Under what conditions, foreshock activity dominates? b) When gouge particles and grooves are created? c) Why precursory slip starts to occur at some point on the fault and expand to both slip perpendicular and slip parallel directions? These key questions will help to solve the rupture dynamics that occurred during the large-scale rock friction experiments.

Keywords: rupture propagation, friction experiments

Crustal deformation and Fault Model for the 2015 Nepal (Gorkha) Earthquake obtained from ALOS-2 SAR Interferometry data

*Tomokazu Kobayashi¹, Yu Morishita¹, Hiroshi Yarai¹

1.GSI of Japan

A devastating earthquake with a moment magnitude (M_w) of 7.8 (USGS) struck central Nepal on April 25, 2015, with its hypocenter located in the Gorkha region. A M_w 7.3 aftershock occurred approximately 150 km east of the hypocenter of the main shock on 12 May 2015, which is the largest aftershock as of this writing. In this presentation, we report the detailed crustal deformation associated with these earthquakes obtained by InSAR analyses and the InSAR-inferred distributed slip model.

We employed a new Japanese L-band synthetic aperture radar satellite launched in 2014, called Advanced Land Observing Satellite-2 (ALOS-2), to measure the ground displacement. ALOS-2 possesses a ScanSAR mode which has an ability to observe over broad area with a swath width of 350 km in one action. The ScanSAR-based InSAR is indeed suitable for mapping the spatially comprehensive and detailed crustal deformation of the 2015 Gorkha earthquake.

We have successfully detected widely distributed ground displacements for the 2015 Gorkha earthquake by applying a ScanSAR-based interferometry analysis. A major displacement area extends with a length of about 160 km in the east-west direction. In the southern/northern part, the displacements moving toward/away from the satellite are observed in both orbits. The main crustal deformation area with ground displacement exceeding 1 m is located 20–30 km east from Kathmandu. A quasi-vertical displacement estimated by combining the ascending and the descending data indicates upheaval of about 1.4 m at maximum.

We inverted the InSAR data including both of the main shock and the largest aftershock to construct a slip distribution model. The fault geometry is assumed to be a plane fault. We set a rectangular fault with 220 km long and 150 km wide, corresponding to the plate interface between the Indian and the Eurasian plates. The fault is divided into square patches with a size of 10 x 10 km. The strike and the dip angles are set to be 290° and 10°, respectively. The major slip occurred with a maximum slip amount of approximately 6.3 m beneath the area 20–30 km northeast from Kathmandu, which is located in 80 km east-southeast of the hypocenter. No significant slip is identified further west from the hypocenter. The seismic rupture is thought to have propagated eastward unilaterally. The slips are nearly pure reverse fault motion, but on the deeper portion have a slight right-lateral component. The spatial extent is zonally distributed within a distance of 50 to 100 km from the surface along downdip direction. The downdip end of the slip is quite consistent with that of the interseismic coupling area geodetically inferred in previous studies. The total estimated moment magnitude including both the main shock and the M_w 7.3 event is 7.8 (seismic moment 7.0×10^{20} Nm). Inverting the InSAR data of pair Nos. 5 and 6 which are for the main shock only and the M_w 7.3 event only, respectively, the estimated moment magnitude is 7.8 (seismic moment 6.1×10^{20} Nm) and 7.3 (seismic moment 1.1×10^{20} Nm), respectively.

The slip distribution unnaturally bifurcates in the east, and we can identify a clear-cut slip deficit area with a radius of ~10 km just west side of the M_w 7.3 event. This area is presumably subjected to a strong shear stress which should promote a reverse fault slip. There is a possibility to produce a fault slip equivalent to M_w ~7.0 in the future although we do not know if the slip heterogeneity would be smoothed out by a seismic event or an aseismic event.

Acknowledgements: ALOS-2 data were provided from the Earthquake Working Group under a cooperative

research contract with JAXA (Japan Aerospace Exploration Agency). The ownership of ALOS-2 data belongs to JAXA. We used ASTER GDEM for the InSAR analyses and the topography mapping. ASTER GDEM is a product of METI (Ministry of Economy, Trade and Industry) and NASA.

Keywords: Crustal deformation, InSAR, Slip Distribution

Frictional properties of materials along Tohoku subduction plate boundaries and implications for fault motion

*Michiyo Sawai¹, André R Niemeijer², Takehiro Hirose³, Christopher J Spiers²

1.Chiba University, 2.Utrecht University, 3.Kochi / JAMSTEC

The 2011 Tohoku-oki earthquake (Mw 9.0) nucleated at 24 km depth along the plate boundary. Moreover, episodic tremor and slow slip events occurred just before the 2011 Tohoku-oki earthquake on a shallow portion (less than 20 km depth) in the Tohoku subduction zone (e.g., Ito et al., 2013). The frictional properties of rocks composed of a subducting oceanic plate exert important controls on the various slip behavior from aseismic to seismogenic slip. However, frictional properties of the rocks to model such subduction earthquakes are poorly understood. We thus conducted friction experiments using a rotary shear apparatus on powders of blueschist (probably distributed at the Tohoku seismogenic zone) and smectite-rich pelagic sediments (present along the shallow portion of the Tohoku plate boundary (Chester et al 2013)). Experiments were performed at temperatures of 20-400°C, effective normal stresses of 25-200 MPa and pore fluid pressures of 25-200 MPa. We investigated the effects of temperature, effective normal stress and slip rate on the rate and state friction parameter ($a-b$) by conducting velocity-stepping experiments with velocity range from 0.1 to 100 $\mu\text{m/s}$.

Blueschist gouges show a positive ($a-b$) values at 22°C which decrease to become negative with increasing temperature. At 200°C, the behavior is velocity weakening and shows negative ($a-b$) values. At 300°C, the gouges show neutral to positive values of ($a-b$), showing larger ($a-b$) values than at 200°C. ($a-b$) values slightly decrease again at 400°C. There is also effective normal stress dependence. The gouges exhibit a transition from velocity-strengthening to velocity-weakening with decreasing effective normal stress. Observed ($a-b$) values decrease with decreasing effective normal stress because of an increase in b with decreasing effective normal stress. Our results suggest that increasing pore pressure is a key factor for nucleating slip leading to both megathrust and slow earthquakes.

In the case of Smectite-rich pelagic sediments, the simulated gouges show negative values of ($a-b$) at low temperatures of 20-50°C, except at the highest slip rate of 0.1 mm/s, and neutral or slightly negative values of ($a-b$) at temperatures of 50-100°C. However, at temperature of >150°C the gouges show positive values of ($a-b$) under almost all velocity conditions tested. The trend of ($a-b$) seems to be identical with that of a , and b shows an inverse relationship with ($a-b$). Slow slip events are considered to be able to nucleate under conditions where ($a-b$) value is negative but close to zero. These conditions are met at temperatures of 50-100°C in our experiments, which is consistent with temperature conditions under which slow slip events occur along the plate boundary at the Japan Trench. The frictional properties of the pelagic sediments explain well the observed distributions of slow slip events in Tohoku subduction zone.

Periodic slow slip and megathrust zone earthquakes in northeastern Japan

*Naoki Uchida¹, Takeshi Iinuma², Robert Nadeau³, Roland Bürgmann³, Ryota Hino¹

1.Graduate School of Science, Tohoku University, 2.Japan Agency for Marine-Earth Science and Technology, 3.University of California, Berkeley

Both aseismic and seismic slip accommodate relative motion across partially coupled plate boundary faults. In northeastern Japan, aseismic slip occurs in the form of decelerating afterslip following large interplate earthquakes and as relatively steady slip on uncoupled areas of the subduction thrust. Here we report on a new quasi-periodic slow-slip behavior that is widespread in the megathrust zone. The repeat intervals of the slow slip range from 1 to 6 years and often coincide with or precede clusters of large ($M \geq 5$) earthquakes, including the M9 Tohoku-oki earthquake. The examination of the spatio-temporal distribution of small repeating earthquakes with respect to the $M \geq 5$ earthquakes suggests that the slow-slip pulses trigger the $M \geq 5$ seismicity. These results suggest that inherently periodic slow-slip events result in periodic stress perturbations and modulate the occurrence time of larger earthquakes. The periodicity in the slow-slip rate has the potential to help refine time-dependent earthquake forecasts.

Keywords: slow slip, repeating earthquakes, interplate earthquakes

Coseismic and postseismic deformation and a fault model of the 2014 Northern Nagano Prefecture Earthquake

*Hiroshi Yarai¹, Tomokazu Kobayashi¹, Yu Morishita¹, Mikio Tobita¹, Shinya Yamada¹

1.Geospatial Information Authority of Japan

Coseismic deformation derived from the 2014 northern Nagano Prefecture earthquake (Mj6.7) was observed by GPS stations of the permanent GPS Earth Observation Network system (GEONET) and ALOS-2/PALSAR-2 interferometric SAR.

We used ALOS-2/PALSAR-2 data acquired by both right and left look direction from descending orbits and right look direction from ascending orbit. The interferograms suggest that fault motion of the earthquake has reverse dip slip with left-lateral motion on an east dipping plane. The most concentrated crustal deformation is located in the southern part of rupture area near epicenter of the mainshock, showing displacements toward to the satellite with ~1 m at the maximum. Clear displacement discontinuity is recognized along western margin of the large crustal deformation area, which is just on the Kamishiro fault.

We invert the InSAR results with GNSS data to construct slip distribution model of the earthquake. From fringe pattern of InSAR images, we assumed that a fault plane changes dip angle at 2 km depth, low dip angle shallower than 2 km and steep dip angle deeper than 2 km. Our preliminary model shows large (over 1 m) slip on southern part of shallower segment and moderate (~1 m) slip around hypocenter of the mainshock on deeper segment. Both segments demonstrate reverse dip slip with left-lateral motion. On the other hand, no significant slip is estimated on northern part of shallower segment.

Postseismic deformation was detected by GEONET and ALOS-2 InSAR.

Acknowledgements.

The PALSAR-2 data obtained by the ALOS-2 were provided by the Japan Aerospace Exploration Agency (JAXA) through the Agreement between GSI and JAXA. The ownership of PALSAR-2 data belongs to JAXA.

Keywords: 2014 Northern Nagano prefecture earthquake , ALOS-2, InSAR, coseismic deformation, postseismic deformation

3D branching fault simulation for dynamic rupture process of 2014 Northern Nagano Prefecture Earthquake

*Ryosuke Ando¹, Kazutoshi Imanishi²

1.Graduate School of Science, University of Tokyo, 2.National Institute of Advanced Industrial Science and Technology, GSJ

The 2014, M_w 6.2, Northern Nagano Prefecture Earthquake broke the Kamishiro fault, which constitutes the northern end of the Itoigawa-Shizuoka tectonic line (ISTL). Associated with this earthquake, several characteristic phenomena indicate the complex configuration of this earthquake processes, as indicative of immaturity of the fault owing to low activity of ISTL at this end section. One of such is found in the surface ruptures, where the offsets were observed to be nearly 1 m for the southern half of the source area, while such surface ruptures were not identified for the northern half. This surface observation consists with the surface displacement distribution inferred from InSAR analysis, suggesting the large slip areas concentrated at near the ground surface on the southern half and at a deeper depth on the northern half, respectively. The surface break is suggested to be a temporally stable structure for a geomorphologic time scale overlapping preexisting fault scarps, and moreover, cumulative fault slip has found by trenching surveys. Another characteristic observation is that the first motion solution of the focal mechanism exhibits nearly pure strike slip faulting, while the centroid moment tensor does the reverse faulting with considerable a non-double couple component. The focal mechanisms of the foreshocks, aftershocks and the spatial distributions of them show the geometry of the source fault is composed of a dipping main-fault and a nearly vertical branch fault.

In this study, we consider this inferred complex fault geometry and carry out the fully dynamic 3 dimensional rupture simulation to understand the factors controlling the observed spatially and temporally heterogeneous features in the rupture process. We give the constraints of the applied stress based on the stress tensor inversion conducted for the focal mechanisms of small earthquake occurred in this region before this earthquake sequence; the maximum principle stress axis is determined to be horizontal oriented at ENE-WSW as the overall direction of the main-fault strike is nearly N-S. The determined stress ratio $(S_2-S_3)/(S_1-S_3)$ is also considered as a constraint together with the assumption of the vertical stress is in the lithostatic condition.

For the numerical simulation, we employed newly developed efficient algorithm for the 3D dynamic boundary integral equation method, called the First Domain Partitioning Method (FDPM) (Ando, 2016, submitted). This method allow us to fully consider the 3D fault geometry together with the ground free surface effect. Each run of the simulation is completed in a few minutes with 48 cores and 15 GB of memory for the following model size: element sizes ~ 0.5 km, number of elements $\sim 2,000$ and time steps ~ 400 .

We performed a series of parameter studies over the stress states concerning its uncertainty in the dynamic rupture simulation. We found, under a certain range of parameter sets, the rupture initiated on the vertical branch fault and then propagated to the dipping main-fault. We further obtained the slip distribution, which is dominated by the strike slip component on the branch-fault and by the reverse components on the main-fault as expected from the orientations of the faults and the principle stresses. In these cases, the reverse faulting slip shows the maximum on the shallow part of the main-fault above the hypocenter, presenting the similarity with the emergence of the observed surface break. The vertical branch-fault existing below the main-fault on the foot wall side seems to contribute the large slip at a depth on the northern half of the source area.

Keywords: Northern Nagano Prefecture Earthquake, 3D fault geometry, Dynamic rupture propagation simulation

Verification of unstable sliding behavior during dehydration of clay minerals as elevated temperature

*Tatsuro Kubo¹, Ikuo Katayama¹

1.Department of Earth and Planetary Systems Science Hiroshima University

Along plate boundary subduction thrusts, the transformation of smectite to illite within fault gouge at temperatures around 100 - 200 °C is one of the key mineralogical changes thought to control the updip limit of seismicity (Hyndman et al., 1997). Ikari et al. (2007) suggest that decreasing water content may contribute to transition from velocity-strengthening to velocity-weakening behavior. Although they analyzed the velocity dependence of clay materials over a wide range of normal stresses and estimated the effect of hydration state on friction properties, their friction experiments were performed with controlling its water content. In the fact that hydration state of clay minerals is possible to vary from moment to moment in nature, systematic studies to investigate the effect of dehydration and hydrate state on frictional properties with progression of a removal of water is rare. In this study, we focus on the effect of dehydration of water on the frictional properties of clay minerals, and compare the results during dehydration process undergoing.

For the friction experiments, starting materials we used are Ca-montmorillonite (CaMMT). The powder materials of clays were placed on the simulated fault surface and two side blocks were placed together to produce a double-direct shear configuration. Normal stress was applied via a hydraulic ram on the side block with 60 MPa, and then, shear stress was applied by advancing the central block downward at a constant velocity. The sample assembly was heated by an external furnace up to 400 °C that is monitored by thermocouples located in the central part of sample assembly. We started to elevate the temperature around the specimen at a constant heating rate of 1, 3, and 10 °C/min, reaching after steady-state friction at 5 mm deformed. Then, we observed friction behavior of CaMMT during dehydration as elevated temperature. Because of the limitation of total displacement to 20 mm in our assembly, we used different slip rate 0.6, 1.2, and 3.0 μm/s at a heating rate 1, 3, and 10 °C/min, respectively.

CaMMT gouge showed unique friction behavior development as elevated temperature at a heating rate of 10 °C/min, which is divided into three stages; friction coefficient decreased at relative low temperature (1), friction coefficient increased at middle temperature (2), and stick-slip behavior occurred at high temperature (3). Stick-slip behavior as elevated temperature implies to have a potential of velocity weakening behavior. However, observed stick-slip behavior occur at a temperature of 324 °C, which is extremely higher from a temperature range of occurring dehydration for CaMMT (100 - 200 °C). We also performed subsequent experiments that heat gouge layer more slowly, using other heating rate; 1 and 3 °C/min. CaMMT gouge at a heating rate 1 °C/min showed similar friction behavior development to that of development at 10 °C/min, divided into three stages as described above. However, the temperature that stick-slip behavior occur shifted to lower temperature, 193 °C. If temperature controlled frictional behavior, the temperature of starting to occur stick-slip behavior is independent of heating rate, and there could be the threshold of temperature starting to exhibit unstable sliding. The observed systematical shift suggest that these frictional behavior is not controlled by temperature, but progression of dehydration. Each friction stages are related to dehydration process, at a first stage friction coefficient decreased because of generation of pore pressure during dehydration. At a second stage, friction coefficient

increased because of a removal of interstitial water, and at a third stage stick-slip behavior occurred when stiffness of gouge layer satisfies a given relationship (Rabinowicz, 1956). Dehydration of clay minerals is intimately connected to friction behavior, and it may have a possibility to trigger seismic friction.

Keywords: effect of dehydration, friction property, clay minerals, elevated temperature, stick-slip

Triggering and driving mechanisms of earthquake swarm

*Teruo Yamashita¹

1. Earthquake Research Institute, University of Tokyo

Earthquake swarms usually occur in volcanic areas, geothermal fields and oceanic ridges. Detailed seismological observations suggest that swarm activity is driven by the flow of fluid, at least, at an initial stage of activity (e.g., Yukutake et al., 2011). Hence, it is believed that high-pressure fluids are involved in the generation of earthquake swarm. However, recent geodetic observations suggest a possibility that aseismically evolving fault drives earthquake swarm activity (e.g., Takada and Furuya, 2010). Aseismic slip is, however, known to be induced by the injection of high-pressure fluid (e.g., Scotti and Cornet, 1994), so that aseismic slip evolution may be related to the existence of high-pressure fluid. It will therefore be indispensable to assume high-pressure fluid in the modeling of earthquake swarm. We may be able to consider the following two contrasting models (models 1 and 2) for the triggering and driving of earthquake swarm if the medium is saturated with fluid. Substantial local pressurization of pore fluid is assumed in model 1. If the crustal stress is near a critical level, ruptures triggered by the fluid pressurization will soon begin unstable growth according to linear fracture mechanics. Such ruptures will be regarded as ordinary earthquakes. Hence, we will have to assume highly under-stressed media and long-sustained supply of high-pressure fluid in model 1. However, model 1 has a weakness that how aseismic slip evolution is coupled with swarm activity is not clear. Although we do not assume local pressurization of fluid or highly under-stressed media in model 2, the fault zone is assumed to be permeated with high-pressure fluid. In such model, we will have to introduce some mechanism to suppress the accelerated rupture growth. One of the mechanisms that have strong compatibility with the existence of high-pressure fluid will be slip-induced dilatancy coupled with fluid flow, which is introduced in model 2. If the slip-induced dilatancy plays a dominant role, we do not necessarily require the local pressurization of fluid to trigger earthquake swarm. What is required for the triggering is the occurrence of small-size seed event. Fluid pressure lowers suddenly in the slip zone concurrently with the occurrence of the seed event if the degree of slip-induced dilatancy is large enough. Since the decrease in the fluid pressure raises the friction, the seed crack does not begin the growth soon after the nucleation. However, the dilatancy induces the fluid inflow from the surrounding medium, which gradually elevates the fluid pressure in the slip zone. This can trigger and drive the aseismic extension of slip zone if the stress state is near a critical level. The rate of aseismic extension depends on the balance between the fluid inflow rate and degree of slip-induced dilatancy. Spatial heterogeneity in the degree of slip-induced dilatancy or fracture strength gives rise to small-scale dynamic events, which will be a model for seismic swarm activity. We theoretically study the generation mechanism of earthquake swarm, assuming model 2, in this study. We analyze quasi-static extension of 2D crack in a linear poroelastic medium saturated with fluid. The dilatancy is assumed to increase with the slip evolution. We assume near-critical stress state, Coulomb's friction coupled with the effective normal stress and Darcy's law for the fluid flow. Our calculation shows that the moment evolution is proportional to $t^{1/2}$ for any values of the model parameters, which contrasts with the classical solution for dynamic crack growth, which is proportional to t^2 (Kostrov, 1964), where t is time. The expansion rates of aseismic slip zone are larger for higher diffusivities and lower degree of dilatancy. If the slip-induced dilatancy is locally negligible, small-scale dynamic slip is triggered at the advancing edge of aseismic slip zone, which is regarded as the occurrence of seismic event.

Keywords: earthquake swarm, fluid, dilatancy

A Source Inversion Method with Realistic Error Model

*Amato Kasahara¹, Yuji Yagi²

1.Graduate School of Life and Environment Sciences, University of Tsukuba, 2.Faculty of Life and Environmental Sciences, University of Tsukuba

Use of a proper likelihood function through incorporation of modeling error and a realistic noise model are essential part of a source inversion analysis, because the shape of the likelihood function affects choice of hyperparameters, the maximum a posteriori (MAP) estimate and its uncertainty estimate. We propose an empirical Bayes method for kinematic linear source inversion with physically based modeling error and realistic noise covariance.

The colored noise effects have been incorporated into analyses of Interferometric Synthetic Aperture Rader (InSAR) and global navigation satellite system (GNSS) data. Recently, effects of colored noise for centroid moment tensor (CMT) inversion were also discussed. However, the colored noise effects were usually ignored in source inversion analyses. In the proposed method, a noise covariance matrix is constructed from continuous records before P arrivals and uncertainty of phase picking.

In earlier studies, both amplitude of noise and a weight of a priori information were treated as hyperparameters. In the proposed method, we reformulated the marginal likelihood function to use the known noise covariance matrix estimated from data before P arrivals and phase picking errors. As we are not able to know the true Earth structure, the calculated Green's functions contain modeling error, and incorporation of the modeling error is unavoidable for the source inversion analysis. Preceding studies approximated effects of modeling error by additional multivariate Gaussian noise (model noise) for data. One of the advantages of the previous approach is its simplicity. As a posterior probability distribution should still be a multivariate normal distribution, MAP estimation and its uncertainty estimation are straightforward. However, even when assuming multivariate Gaussian error for the elements in the coefficient matrix, it is shown that the theoretical likelihood function is a skewed function and not a multivariate normal distribution function. Thus, the previous approach biases the MAP estimate and potentially affect choice of hyperparameters. We propose another approach, which does not use model noise approximation, to incorporate effects of modeling error into source inversion analysis. In the present approach, the Earth structure is assumed to be a random variable, which follows a known probability distribution. Then, the Earth structure is marginalized to obtain a posterior probability distribution of the source process. The proposed approach naturally incorporates associations of modeling errors for different type of data (e.g. seismic waveforms and surface displacements). As the marginalization is not analytically possible in most cases, we use a Monte-Carlo method and obtain the posterior probability distribution as a finite mixture of multivariate normal distributions. The MAP estimate is obtained by using a numerical optimization technique.

Keywords: Source inversion, Empirical Bayes method, Modeling error

Statistical Properties of the Olami-Feder-Christensen Model on the Complex Network

*Hiroki Tanaka¹, Takahiro Hatano¹

1. Earthquake Research Institute, Tokyo University

As a statistical model of seismicity, Olami-Feder-Christensen (OFC) model, which is thought to represent the stress distribution on the fault plane, has been studied and found that the model reproduces statistical properties similar to the real earthquakes including Gutenberg-Richter law and Omori formula for aftershock sequence. In most cases, OFC model has been studied on two-dimensional lattice, and the system is uniform in the sense that the cells are under the same condition. On the other hand, it is well known that earthquakes occur spatially non-uniformly. Recent studies showed that the network constructed by connecting the epicenters of successive earthquakes behaves as a Barabasi-Albert (BA) type scale-free network. Therefore in this study we simply incorporate such a spatial non-uniformity by thinking the OFC model on BA scale-free network and examine the statistical properties. This model includes two parameters; one is for the model construction, and the other is the dissipation-rate between nodes during stress redistribution. We mainly study the dissipation-rate dependence of statistical properties.

As a result, it is found that the magnitude frequency obeys nearly power law as well as the GR law, regardless of the dissipation-rate. Furthermore, by changing the dissipation-rate, the statistical behavior varies and is roughly categorized into three types; (1) Mainshock-Aftershock, (2) Foreshock-Mainshock-Aftershock, and (3) Stationary sequences. Especially first two behaviors are similar to the characteristic intermittent-clustering behavior of earthquakes.

Characteristic feature of this model is that even if the node has largest degree, sometimes multiple-releases occur in one event. During such a large event (regarded as the mainshock) stress redistribution is repeated between large degree nodes and overwhelmingly many smaller nodes. Therefore, as almost all nodes in the network are involved in the mainshock, aftershocks in this model are not considered to be the events releasing the remaining stresses which are not released by the mainshock.

In order to understand the role of aftershocks in this model, we propose a roughness parameter, which is thought to reflect the non-uniformity of stresses on the network, to make clear the total behavior of OFC model. With this parameter we found that aftershocks are not thought to be the events in order to release remaining stress at the edge of the mainshock rupture zone, but to be the process that nodes interact and cooperate to return to a stable roughness level specific to the construction of the network.

Unexpectedly rapid decrease of meter-sized rock friction at high work rate

*Futoshi Yamashita¹, Eiichi Fukuyama¹, Kazuo Mizoguchi², Shigeru Takizawa¹, Shiqing Xu¹, Hironori Kawakata³

1.National Research Institute for Earth Science and Disaster Prevention, 2.Central Research Institute of Electric Power Industry, 3.Ritsumeikan University

We here report rapid decrease of meter-sized rock friction at high work rate revealed by large-scale biaxial experiments at NIED. In the experiments, we used a pair of meter-sized Indian metagabbro as specimens, whose contacting area was 1.5 m long and 0.1 m wide. The experimental conditions were normal stress up to 6.7 MPa and loading velocity up to $3 \times 10^{-2} \text{ ms}^{-1}$. We confirmed the work rate dependency of rock friction as previously reported with centimeter-sized experiments (Di Toro *et al.*, 2011, Nature), but further found that the meter-sized rock friction starts to decrease at a work rate of $10^{-1} \text{ MJm}^{-2}\text{s}^{-1}$, which is one order of magnitude smaller work rate (still high in absolute sense) than that of the centimeter-sized one. After each meter-sized experiment, we found localized damages (i.e. grooves) were generated on the fault surface and gouge materials were distributed in and around them. Especially, we often found heavily comminuted gouge in the grooves, which swelled up relative to the surrounding fault surface. Mechanical, visual and material observations suggest that slip-evolved stress heterogeneity on the fault accounts for the differences of frictional properties between meter and centimeter sizes. Based on these observations, we propose that slightly stress-concentrated areas pre-exist in which frictional slip produces more gouge than in areas outside, resulting in further stress concentrations at these areas. The overall shear stress on the fault is primarily sustained by the stress-concentrated areas that undergo a work rate higher than the average, so those areas should weaken more rapidly and cause the macroscopic frictional strength to decrease abruptly. To verify this idea, we conducted numerical simulations assuming that local friction follows the frictional properties observed on centimeter-sized rock specimens. The simulations reproduced the macroscopic frictional properties observed on the meter-sized rock specimens. This result suggests the rapid reduction of macroscopic frictional strength at the work rate lower than the expected one with centimeter-sized results should be taken into consideration, since such slip-evolved heterogeneity should be common in nature. Further details related to this presentation can be found in Yamashita *et al.* (2015, Nature).

Keywords: Rock friction, Scale dependence, Work rate

Detection of frictional heating on faults using Raman spectra of carbonaceous material

*Kohtaro Ujiie^{1,2}, Hiroki Tabata¹, Yui Kouketsu³, Hiroyuki Kagi⁴, Weiren Lin⁵

1.Graduate School of Life and Environmental Sciences, University of Tsukuba, 2.Research and Development Center for Ocean Drilling Science, Japan Agency for Marine-Earth Science and Technology, 3.Graduate School of Environmental Studies, Nagoya University, 4.Geochemical Laboratory, Graduate School of Science, University of Tokyo, 5.Kochi Institute for Core Sample Research, Japan Agency for Marine-Earth Science and Technology

The detection of frictional heating on faults is a key to assessing coseismic shear stress and frictional work during earthquakes. Raman spectra of carbonaceous material (RSCM) have been widely used as a geothermometer on sedimentary and metamorphic rocks. We examined whether RSCM can be useful to detect increased temperatures associated with frictional heating on faults. The studied fault rocks are a few millimeters-thick pseudotachylyte derived from chert, 10 cm-thick cataclasite marked by fragments of chert in the carbonaceous mudstone matrix, and ~1 mm-thick pseudotachylyte derived from argillaceous rock, which are distributed in the exhumed accretionary complexes in the Mino-Tamba and Shimanto Belts, Japan. The results indicate that the intensity ratio of D1 and D2 Raman bands (I_{D1}/I_{D2}) markedly increase in pseudotachylytes, while increased I_{D1}/I_{D2} is absent in the cataclasite. The increased I_{D1}/I_{D2} values in pseudotachylytes are considered to represent coal maturation associated with increased heating along the localized slipping zone of less than a few millimeters thick. The absence of increased I_{D1}/I_{D2} values in the cataclasite may reflect the restricted temperature rise, which is consistent with distributed shearing along the 10 cm-thick slipping zone. The I_{D1}/I_{D2} values are also increased in the chert within ~2 mm from the upper boundary of the pseudotachylyte and drop to the background level >2 mm away from the upper boundary. In contrast, the increased I_{D1}/I_{D2} values are not observed in the chert below the pseudotachylyte and the argillaceous rocks above and below the pseudotachylyte. The measurements of thermal properties suggest that coal maturation in the chert within ~2 mm from the upper boundary of the pseudotachylyte is attributed to the higher thermal diffusivity in the hanging wall chert relative to the footwall chert and the argillaceous rock. The increased I_{D1}/I_{D2} values in pseudotachylytes and the chert within ~2 mm from the upper boundary of the pseudotachylyte indicate that coal maturation can occur during short-lived thermal events such as frictional heating on faults. Therefore, RSCM is useful to detect frictional heating. However, the conventional RSCM geothermometer cannot apply for the estimation of peak temperature during frictional heating on faults, because the maximum temperature determined from the RSCM geothermometer is well below the minimum temperatures recorded in the pseudotachylytes. The reaction kinetics incorporating the effects of rapid heating is necessary to establish frictional heating thermometer on faults.

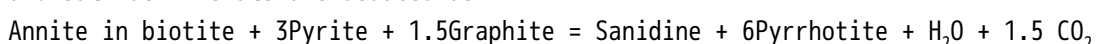
The estimation of redox state based on the fluid-deposited graphite and sulfide minerals in fault rocks

*Yoshihiro Nakamura¹, Madhusoodhan Satish-Kumar², Tsuyoshi Toyoshima²

1. Graduate School of Science and Technology, Niigata University, 2. Department of Geology, Faculty of Science, Niigata University

The redox state in fault rocks provide valuable information on the physicochemical properties related to the fluids during seismic activity (O'hara and Huggins, 2005). However, there are very few studies on direct clues for fluid activities obtained from fluid inclusion (Boullier et al. 2001) and estimation of fluid contents using micro-FTIR (Famin et al. 2008). It is usually difficult to distinguish between syngenetic and postgenetic fluid activities from altered and hydrated fault rocks and pseudotachylytes that indicate paleo-seismic activity (Kirkpatrick and Rowe 2013).

Here we focus on carbon- and sulfur-bearing minerals in fault zones in order to understand the dynamic changes of oxygen fugacity (fO_2) and sulfur fugacity (fS_2). The study area, located in the Hidaka metamorphic belt, Hokkaido, Japan, is a metasedimentary unit where cataclasites, ultracataclasites and two different types of pseudotachylytes; Pst I and Pst II are distributed. Pyrrhotite ($N[FeS] = 0.92-0.94$) + Kfs assemblage is found in Pst I matrix, whereas biotite microlite + Kfs assemblages with fluid deposited graphite is only found in Pst II matrix. The fluid deposited graphite is only observed in the Pst II matrix, which was generated at around 1200 degree C, and characterized by the breakdown of plagioclase and apatite. The carbon isotope composition of the fluid deposited graphite were between -18.2 and -25.4 permil, shifting the carbon isotope values of +2 ~ +3 permil from the metamorphic graphite in protolith, cataclasite and Pst I. Our observations suggest that the graphite and sulfide minerals converted to COHS fluids by frictional melting, and then reprecipitate as secondary minerals under favorable fO_2 - fS_2 environments. In order to assess the redox state, we attempt to estimate the P - T - fO_2 - fS_2 phase diagram during frictional melting. The thermal decomposition of biotite coexisting with graphite and sulfide minerals are deduced as:



The breakdown of biotite changes the redox state to the more oxidation state at ranges between $\delta \text{FMQ} +0.5 \sim +3.0$. Under a high-temperature condition (> 1200 degree C), biotite microlite + Kfs with fluid deposited graphite are usually observed instead of pyrrhotite in pseudotachylytes. This suggests the negative shift to biotite stability field by lowering fS_2 and fO_2 . In addition, using the positive 2~3 permil shift by carbon isotope fractionation, the calculated $x\text{CO}_2$ ($= \text{CO}_2 / (\text{CH}_4 + \text{CO}_2)$) ranges between 0.12 and 0.03. The calculated fO_2 is evaluated between -21.6 and -22.0 \log_{10} units, suggesting the CH_4 dominant fluid based on the estimated ideal fluid mixing model. When the fluid composition encounters the graphite saturation surface in COH diagram by supersaturation, the fluid deposited graphite begins to precipitate with hydrous silicates such as hydroxyapatite and titanite, and shift the large carbon isotope fractionation by small fluctuation in $x\text{H}_2\text{O}$. Such precipitation model is in good agreement with the microtextural observations in pseudotachylyte matrix. The most important implication of our finding is that the redox state in both types of pseudotachylytes are controlled by graphite breakdown. Our finding of fluid deposited graphite in pseudotachylytes suggest that sediments can produce the COHS fluids by frictional melting and the graphite play as a reducing agent in fault rocks.

References: Boullier et al. (2001), JGR, 106, 21965-21977. Famin et al. (2008), EPSL, 265, 487-497. Kirkpatrick and Rowe, (2013), JSG, 52, 183-198. O'hara and Huggins (2005), CMP, 148, 602-614.

Keywords: Graphite, Stable carbon isotope , Pseudotachylyte, Redox state

Aftershock distribution and focal mechanisms of 2014 M_w 5.4 Orkney earthquake, South Africa, by using underground seismic networks in gold mines

*Kazutoshi Imanishi¹, Hiroshi Ogasawara², Yasuo Yabe³, Shigeki Horiuchi⁴, Makoto OKUBO⁵, Osamu Murakami⁶

1.Geological Survey of Japan, AIST, 2.Faculty of Science and Engineering, Ritsumeikan University, 3.Research Center for Prediction of Earthquakes and Volcanic Eruptions, Graduate School of Science, Tohoku University, 4.Home Seismometer Corporation, 5.National Science Cluster, Kochi University, 6.Tono Research Institute of Earthquake Science, Association for the Development of Earthquake Prediction

The M_w 5.4 Orkney earthquake occurred on August 5, 2014, near Orkney town, South Africa. The mainshock and aftershocks were recorded by underground networks in gold mines, which are composed of 46 three-component geophones installed at 2-3 km depths. The sampling rate is 6 kHz. The observed waveforms have high signal-to-noise ratios and contain higher frequency components up to at least 1 kHz, which provide the opportunity for precise determination of aftershock distribution and source parameters. We determined hypocenters of 2000+ aftershocks by automatic earthquake location software from Home Seismometer Corp. (Horiuchi et al., 2011). Aftershocks distributed at depths from about 4 to 7 km forming a 8 km-long in the NNW-SSE direction. The distribution agrees with one of nodal planes of the mainshock focal mechanism, suggesting that the mainshock represents a left lateral strike-slip fault. Aftershock focal mechanisms were determined from P-wave polarity data as well as body wave amplitudes. As a preliminary analysis, we analyzed aftershocks with at least 15 P-wave polarities and obtained 137 well-determined solutions. Most of aftershocks show a pure strike-slip mechanism that is similar to the mainshock. We also found some aftershocks whose P- and T- axis deviates from the general trend and contain normal or reverse faulting components. These events seem to distribute at the middle and the north of the aftershock distribution, suggesting the existence of local stress heterogeneity. Further analysis of aftershocks is needed to elucidate whether the heterogeneity was caused by stress changes due to the mainshock and/or associated with locally formed pre-mainshock stress regime.

Acknowledgements. The seismic network used in this study is operated by AngloGold Ashanti and Open House Management Solutions. The data processing was performed by Institute of Mine Seismology. The data ownership belongs to AngloGold Ashanti.

Keywords: 2014 M_w 5.4 Orkney earthquake , Gold mines, South africa, Aftershock distribution, Focal mechanism

Responses of Stick-Slip Oscillator to Periodically External Forces (2)

*Kazuro Hirahara¹

1. Department of Geophysics, Earth and Planetary Sciences, Graduate School of Sciences, Kyoto University

There have so far been a large number of studies on statistical significance of periodicity and seasonality of seismic activities. Recently, some studies have proposed physical mechanisms causing such periodicity and seasonality. For example, the following studies have been executed: stress perturbation on faults causing some correlation between seismic activity and Earth-Ocean tide (Tsuruoka & Ohtake, 2002); correlation between activity of low frequency earthquakes and oceanic tide (Nakata et al., 2008) and proposal of its nonlinear response (Ide & Tanaka, 2014); correlation between large earthquake activity and long-term lunar tide (8.85 years) and amplification mechanism of lunar tide (Tanaka, 2014); seasonality of Nankai trough earthquake occurrences (Mogi, 1969; Ohtake & Nakahara, 1999) and correlation between long-term lunar tide (18.61 years) and their occurrences (Ide & Tanaka, 2014). Recently, Uchida et al. (2016) reported the existences of 1-6 year periodicities of repeating earthquake activities on the Pacific plate interface and their triggering large earthquakes.

As stated above, there exist some periodicities of slip behaviors ranging from slow slips to large earthquakes. And earthquakes occurring on plate interfaces and inland faults have some rhythms of recurrence intervals called earthquake cycles and co-rupturing of some earthquakes. We may consider the former periodicities as responses of stick-slip oscillator to periodic forces such as earth and ocean tides, and the latter earthquake cycles as interaction of coupled stick-slip oscillators in asperities and the co-rupturing as synchronization of asperity ruptures. Following these ideas, I started to explore the possibility of constructing a new model of earthquake activities and cycles, by both employing earthquake cycle simulations following rate-state friction law and synchronization theory developed in non-linear sciences (e.g., Kuramoto, 1984).

Sugiura et al. (2014) investigated synchronization of coupled stick-slip oscillators following rate-state friction. There have been, however, no studies on responses to external forces. Therefore, Hirahara (2015, SSJ Fall meeting) investigated the responses of 1 degree of freedom stick-slip oscillator to external forces. This talk is a follow-up report.

Hirahara (2015) found $m:n$ synchronization phenomena, which is usually called as Devil's Staircase, in cases of applying periodic external stresses with the amplitudes of $1/10$ and $1/100$ relative to the whole stress changes in stick-slip cycles. Here, $f_e:f_c=m:n$ (m and n are coprime integers) where f_e and f_c are frequencies of external force and simulated system, respectively. Earth and ocean tidal loading has stress with the amplitude of kPa-10kPa, and such loading may cause synchronization of SSE with small stress changes of several 100 kPa.

In this talk, I try to explain $m:n$ synchronization and its synchronization width by employing simulated phase response curves. Then, I show the responses to external forces with not single but multiple frequencies, and also the responses to forces based on actual earth and ocean tidal models. Further, I report another interesting phenomena of non-synchronization, where the intervals of slip increasingly varies, especially in range of the larger external periods outside of $m:n$ synchronization. These phenomena may be related to the observed fluctuations of periodicity of earthquake activities and cycles.

Keywords: Stick-Slip Oscillator, Synchronization, Rhythm, External Force, Earthquake Cycle Simulation

Frictional properties of mafic metamorphic gouges: Implication for slow earthquakes along the Nankai Trough

*Ayumi S. Okamoto¹, André R. Niemeijer², Christopher J. Spiers², Toru Takeshita¹

1. Graduate School of Science, Hokkaido University, 2. Faculty of Geosciences, Utrecht University

Both megathrust earthquakes and slow slip events have occurred at similar depth of ~30 km along the Nankai Trough, near southwest Japan. A convergent subduction boundary consists of kinds of materials such as sediments constituting an accretionary prism and mafic/ultra-mafic rock constituting crust and upper mantle. In order to understand the mechanisms relevant to subduction zone earthquakes, and to discuss the effect of physical conditions such as temperatures (T) and pore pressure ratio (λ), we need to know the mechanical properties of these rocks. In this study, we investigate frictional properties of mafic rocks constituting the oceanic crust. Note that the mafic rocks have been gradually and partially transformed to metamorphic rocks by metamorphism. The oceanic crust at the uppermost part of the Philippine Sea plate subducting along the Nankai Trough, might have been transformed by metamorphisms into prehnite-pumpellyite (PP), prehnite-actinolite (PA) and greenschist (GS) facies (~10-20 km depth) rocks, and epidote-blueschist (eBS), epidote-amphibolite (eAM) and GS facies (~20-30 km depth) rocks, based on the metamorphic facies diagram from Hacker *et al.* (2003) and the temperature-depth profile calculated by Yoshioka *et al.* (2013). Observation of natural deformation texture of GS and BS rocks shows that fine-grained actinolite (Act) and chlorite (Chl) mixture fills up a space between relatively coarse-grained amphibole, epidote, clinopyroxene and opaque minerals. These fine-grained aggregates are deformed to a large strain accommodated by coupled micro-fracturing and pressure solution. Other dominant minerals (e.g. epidote), however, seem to be little deformed, and behave as rigid bodies. Based on the observation, mentioned above, we performed hydrothermal ring shear experiments using a mixture of actinolite (Act, ~85%) and chlorite (Chl, ~15%) at effective normal stresses (σ_n^{eff}) of 50-200 MPa, pore fluid pressures (P_f) of 50-200 MPa, T of 22.5-600°C, and sliding velocities (V) of 0.0003-0.1 mm/s. Our results show that the rate- and state-dependent friction parameter ($a-b$) is affected by both σ_n^{eff} and P_f at $T = 200-400^\circ\text{C}$. At low velocity-step (e.g. 0.0003-0.001 mm/s), ($a-b$) shows negative at this temperature range, whereas it increases to positive with increasing V . To extrapolate the results of the mechanical behaviors outside the experimental conditions, we quantify the effects of σ_n^{eff} and P_f on ($a-b$) in the lowest velocity-step from 0.0003 to 0.001 mm/s, using a multiple regression analysis. By applying the results of these empirical fits to the P - T conditions of the Nankai Trough, we demonstrate that a high $\lambda(P_f / (\sigma_n^{\text{eff}} + P_f))$, pore pressure ratio) above ~0.92-0.95 is needed for unstable, velocity-weakening behavior on Act + Chl gouge. However, since ($a-b$) increases with increasing V , unstable slip nucleating in a mixture of Act + Chl, can transition to stable sliding with increasing V , and stop without developing a huge rupture event. Act + Chl gouges therefore might have slipped at low velocity, resulting in slow earthquakes concentrating stress in adjacent undeformed bodies (i.e. asperities) of different assemblages and texture.

Keywords: metamorphic rock, oceanic crust, frictional behavior, Nankai Trough, amphibole, pore pressure ratio

Correlation between frictional properties and deformation textures in frictional experiments on the biogenic sediment collected from the oceanic plate offshore Costa Rica

*Yuka Namiki¹, Akito Tsutsumi¹

1. Graduate School of Science, Kyoto University

Various seismic behaviors such as large earthquakes, episodic slow slip events, or silent earthquakes are observed in subduction zones. This variation likely reflects spatial variations in frictional properties along the seismogenic portion of plate-boundary megathrusts (e.g., Bilek and Lay, 1998). A number of studies revealed frictional properties of clay sediments collected from the Nankai Trough (e.g., Brown, 2003). However, available experimental data have been limited mostly to clayey subduction-zone materials. In this study, to reveal the frictional properties of the biogenic sediments, we performed a series of friction experiments on silicic to calcareous ooze. The samples tested in this study were collected at a reference site of offshore Costa Rica (Site U1381) during the IODP expedition 334 and 344.

Namiki et al. (2014) have shown that the frictional properties of the silicic to calcareous ooze were different from those of the clay sediments as the following: (1) the steady-state μ values of the silicic to calcareous ooze are high, measuring 0.6 to 0.8; and (2) the μ values of the silicic to calcareous ooze samples show negative velocity dependence of friction at velocities of 0.0028 to 0.28 mm/s and positive velocity dependence at velocities of 0.28 to 2.8 mm/s. The second property is important because velocity-weakening behavior implies potentially unstable fault motion.

To understand the mechanism of generating such characteristic frictional properties of the silicic to calcareous ooze, a series of friction experiments were performed on biogenic amorphous silica as an end-member component of the silicic to calcareous ooze. We dissolved calcite by acid treatment, and gained amorphous silica whose particle size and shape were similar to natural sediments. The biogenic amorphous silica shows the following frictional properties: (1) the steady-state μ value is high, measuring ~ 0.6 , and (2) the biogenic amorphous silica shows negative velocity dependence of friction at velocities of 0.0028 to 2.8 mm/s. The first property suggests the frictional steady-state strength of the biogenic amorphous silica is similar that of the silicic to calcareous ooze. The second property suggests mixing amorphous silica and calcite probably influences positive velocity dependence of friction of the silicic to calcareous ooze at velocities of several mm/s. Microstructures of the sheared samples are observed by SEM. The silicic to calcareous ooze, which displays positive velocity dependence of friction at velocities of 0.28 to 2.8 mm/s, shows distributed deformation texture. The silicic and calcareous shells show preferred orientation inclined to the shear zone at an angle in the range of about 30°. Both distributed and localized deformation textures are observed for the amorphous silica sample, which shows negative velocity dependence of friction at velocities of 0.0028 to 2.8 mm/s. Preferred orientation of silica grains characterizes the distributed deformation textures. Two types of localized deformation textures are observed: zones of random fabric and shear fractures. In the random-fabric zones, silica grains are rounded. The rounded silica does not show the typical shape of the shells. The shear fractures intersect with the shear zone at an angle in the range of 10° to 20°. Preferred orientation of the silica grains parallel to the orientation of the shear fractures are observed within one of the shear fractures. Ikari et al. (2013) mentioned the nanofossil chalk, which showed negative velocity dependence of friction, exhibited prominent Riedel shears. It is likely that the localized deformation textures observed in our amorphous silica experiments are Riedel shears.

Keywords: Frictional experiments, Shear structure, CRISP

The effect of heterogeneous crust on earthquakes:a case study of the 2011 North Nagano earthquake

*Takashi Miyatake¹

1.Earthquake Research Institute, University of Tokyo

We investigated the effects of heterogeneous crustal structure on earthquake rupture of the 2011 North Nagano earthquake. Using a 3D crustal structure model (Matsubara et al.,2008) we calculate stress distribution by solving static equation of motion. The finite difference method with grid size of 0.1km is used, where the computational space is 100km x 100km x 50km. Displacement boundary condition is applied. Since absolute value of boundary displacement is unknown, relative values of stress components, and the stress ratio, i.e., (fault shear stress) / (fault normal stress) are discussed. Because (stress ratio) = (stress drop) / (normal stress) -dynamic frictional coefficient, the ration roughly indicates normalized stress drop. We found high stress ratio region seem to be overlapped the fault asperity. It suggests that the earthquake could have been created by a heterogeneous stress field generated from heterogeneous crustal structure.

Keywords: crustal structure, fault stress, asperity

The Effective Stress Law at a Brittle-Plastic Transition: Analogue Experiments with Halite Gouge Layers

*Hiroyuki Noda¹, Miki Takahashi²

1.Japan Agency for Marine-Earth Science and Technology, 2.National Institute of Advanced Industrial Science and Technology

We investigated the effect of pore pressure P_f near the brittle-plastic transition (BPT) for a halite (NaCl) shear zone. Our series of pre-cut friction experiments with a gas-medium apparatus with temperature $T \leq 200^\circ\text{C}$, confining gas pressure $P_c \leq 150$ MPa, and $P_f \leq 140$ MPa revealed that a tanh connection between the brittle and plastic regimes works well even at elevated P_f , with a coefficient for P_f in an effective stress law α being unity. Plastic deformation around the real contacts independent of the mean stress results in $\alpha=1$ regardless of the ratio of the real contact area A_r/A . The functional dependency of the shear strength on the effective normal stress may deviate from a linear dependency with increasing A_r/A . The present findings support a smooth transition in a hypothetical steady-state strength profile around a BPT, providing new insights in geologically obtained paleo-stress data in exhumed mylonitic shear zones.

Keywords: Effective stress law, Brittle-plastic transition, Friction experiment

Rupture process during the 2015 Illapel Chile earthquake: Zigzag-along-dip rupture episodes

*Ryo Okuwaki¹, Yuji Yagi¹

1. Graduate School of Life and Environmental Sciences, University of Tsukuba

We constructed a seismic source model for the 2015 Mw 8.3 Illapel, Chile earthquake, which was carried out with the kinematic waveform inversion method adopting a novel inversion formulation that takes into account the uncertainty in Green's function, together with the hybrid backprojection (HBP) method enabling us to track the spatiotemporal distribution of high-frequency (0.3–2.0 Hz) sources at high resolution by using globally observed teleseismic P-waveforms. A maximum slip amounted to 10.4 m in the shallow part of the seismic source region centered 72 km northwest of the epicenter and generated a following tsunami inundated along the coast. In a gross sense, the rupture front propagated almost unilaterally northward from the hypocenter at less than 2 km/s, however in detail the spatiotemporal slip distribution also showed a complex rupture propagation pattern: two up-dip rupture propagation episodes, and the secondary rupture episode may have been triggered by the strong high-frequency radiation event at the down-dip edge of the seismic source region. High-frequency sources tended to be distributed at deeper parts of the slip area, a pattern also documented in other subduction-zone megathrust earthquakes that may reflect the heterogeneous distribution of fracture energy or stress drop along the fault. The weak excitation of high-frequency radiation at the termination of rupture may represent the gradual deceleration of rupture velocity at the transition zone of frictional property or stress state between the megathrust rupture zone and the swarm area.

Keywords: complex rupture process during megathrust earthquake, backprojection, kinematic waveform inversion

On the magnitude and heterogeneity of crustal stress

*Yoshihisa Iio¹

1. Disaster Prevention Research Institute, Kyoto University

The Magnitude of shear stress in the crust is one of the most important parameters in seismology, however, it has been unknown in a long time. We will infer it from dense seismic data, and further estimate theoretically whether the magnitude is large or small.

Keywords: crustal stress, heterogeneity, seismogenic region